In Vivo Elevation of Mitochondrial Activity and Amyloid Deposition, but Inversely Correlated, in Early-stage Senescence-Accelerated Mice: A Positron Emission Tomography Study

Satoru Yamagishi
Hamamatsu University School of Medicine
Yurika Iga
Hamamatsu University School of Medicine
Shunsuke Ikegaya
Hamamatsu University School of Medicine
Takeharu Kakiuchi
Hamamatsu Photonics K.K.
Hiroyuki Ohba
Hamamatsu Photonics K.K.
Shingo Nishiyama
Hamamatsu Photonics
Masakatsu Kanazawa
Hamamatsu Photonics K.K.
Hideo Tsukada
Hamamatsu Photonics K.K.
Kohji Sato
Hamamatsu University School of Medicine
Yasuomi Ouchi (ouchi@hama-med.ac.jp)
Hamamatsu University School of Medicine

Original research

Keywords: mitochondrial activity, senescence-accelerated prone mouse,mild cognitive impairment, positron emission tomography, immunostaining

DOI: https://doi.org/10.21203/rs.3.rs-27076/v1

Abstract

Background: While marked reductions in neural activity and mitochondrial function have been reported in Alzheimer's disease (AD), the degree of mitochondrial activity in mild cognitive impairment (MCI) or early-stage AD remains unexplored. Here, we used positron emission tomography (PET) to examine the direct relationship between mitochondrial activity (^{18}F-BCPP-EF) and β-amyloid (Aβ) deposition (^{11}C-PiB), followed by immunohistochemistry for ATPB (an ATP synthase on the mitochondrial inner membrane), in the same brains of senescence-accelerated mouse prone 10 (SAMP10) mice, an Aβ-developing neuroinflammatory animal model showing accelerated senescence with deterioration in cognitive functioning similar to that in MCI.

Results: The SUVRs of ^{18}F-BCPP-EF and ^{11}C-PiB were significantly higher in the 15-week-old SAMP10 mice than in the control and 5-week-old SAMP10 mice. The two parameters were found to negatively correlate with each other. Consistent with these binding results, the immunohistochemical analysis demonstrated upregulation of ATPB in neurons, astrocytes, and microglia, but not in pericytes, in the 15-week-old SAMP10 mice.

Conclusions: The present results provide in vivo evidence of an increase in mitochondrial energy production and amyloid burden at an early stage in SAMP10 mice. The inverse correlation between these two phenomena suggests a concurrent compensatory increase in neuronal energy production and Aβ-induced elevation of neuroinflammatory responses in glial cells, as confirmed immunohistochemically. The combination of PET and immunohistochemistry allowed in vivo evaluation of altered mitochondrial activity during neuropathological processes, including Aβ accumulation, in an animal model of AD spectrum disorder.

Introduction

It is well recognized that mitochondrial dysfunction contributes to the neurodegeneration occurring in Alzheimer's disease (AD). Recent findings suggest that pathological changes that occur in AD brains, such as synaptic and neuronal losses and excessive β-amyloid (Aβ) production, may be induced by mitochondrial dysfunction and increased oxidative stress [1]. In AD patients, mitochondria are reportedly characterized by impaired functioning, including lowered oxidative phosphorylation, decreased adenosine triphosphate production (ATP), increased generation of reactive oxygen species (ROS), and compromised antioxidant defense [2]. Mild cognitive impairment (MCI) is an intermediate condition of impaired cognitive function between normal aging and dementia, and is commonly associated with progression to AD [3, 4]. The Aβ deposition rate in patients with MCI who are likely to convert to AD is greater than that in stable patients [5]. However, the *in vivo* relationship between mitochondrial activity and Aβ level in the state of senescence to MCI remains unclear.

We previously developed an ^{18}F-BCPP-EF tracer for mitochondrial complex 1, which provides an experimental advantage in that it allows time-course changes in mitochondrial activation to be studied in

vivo [6]. Specifically, this probe can visualize the availability of complex I, the first component of four electron transport complexes in the inner mitochondrial membrane, and which can be specifically inhibited by rotenone. Using this probe, we successfully monitored dysfunction in mitochondrial activity in a rat cortical ischemia model [7] and in the parahippocampal region of the early-stage human AD brain [8].

SAMPs (senescence-accelerated mouse prones) are inbred mouse lines showing accelerated aging. There are currently nine independent strains from SAMP1 to SAMP11, which show distinct features of the aging phenomenon. Among these lines, the SAMP10 line shows neuronal loss with Aβ deposition, and impairment of learning and memory due to cortical degeneration in later life [9]. At 8–16 months-of-age, not only are the numbers of neurons reduced, but so are the lengths of dendrites and the spine densities of cortical pyramidal neurons [10]. Preceding this neuronal degeneration, microglia are affected at an earlier stage (~ 3 months-of-age) [11], with the number of segments and tips and the combined lengths of microglial processes being significantly decreased. We recently reported that at this stage, during which morphological impairments in microglia occur (i.e., the number of segments and tips and the combined lengths of microglial processes become much reduced), type 2 endocannabinoid receptor (CB2)-positive protective microglia are dominant compared with translocator protein 18 kD (TSPO)-positive inflammatory microglia [12]. Therefore, the merit of using the SAMP10 line at this early stage is that it allows exploration of alterations in molecular events before substantial brain atrophy occurs, which is comparable with the state of the senescence in MCI in humans.

In this study, we used ^{18}F-BCPP-EF and ^{11}C-PiB PET tracers and immunohistochemistry to investigate the in vivo relationship between mitochondrial activity and Aβ deposition in the brains of SAMP10 mice during the early stage of neurodegeneration.

Materials And Methods

Animals

Six 15-week-old senescence-accelerated mouse resistant 1 (SAMR1) mice, which develop normal senescence and are often used as a control line for SAMP mice, and eight 5-week-old and eight 15-week-old senescence-accelerated mouse prone 10 (SAMP10) mice purchased from the SLC Company (Hamamatsu, Japan), were used in this study. The mice were housed with their littermates to a maximum of five animals in each cage with food and water available *ad libitum*. All animal protocols and the following experiments were approved by the ethics committees of the Central Research Laboratory at Hamamatsu Photonics and Hamamatsu University School of Medicine. In addition, all applicable institutional and/or national guidelines for the care and use of animals were followed.

Tracer production

PET Ligand Syntheses

The HM-18 cyclotron (Sumitomo Heavy Industry, Ltd., Tokyo, Japan) situated at Hamamatsu Photonics PET center was used to produce the positron-emitting radionuclides ^{11}C and ^{18}F in $^{14}N(p,\alpha)^{11}C$ and $^{18}O(p,n)^{18}F$ nuclear reactions, respectively. The labelled compounds were then synthesized with a modified CUPID system (Sumitomo Heavy Industries, Ltd., Tokyo, Japan). ^{18}F-BCPP-EF was radiolabeled by nucleophilic ^{18}F-fluorination of the corresponding precursor, as described elsewhere [6, 7]. The radiochemical purity was more than 99% and the specific radioactivity was above 50.0 GBq/μmol. ^{11}C-PiB was synthesized by N-methylation of the nor-compound N- desmethyl-PIB with ^{11}C-methyl triflate [13]. The radiochemical purity was more than 96% and the specific radioactivity was above 35 GBq/μmol.

PET measurements

PET was performed using a high-resolution animal PET scanner (SHR-38000, Hamamatsu Photonics, Hamamatsu, Japan) with an axial field of view (FOV) of 108 mm, a transaxial FOV of 330 mm, and a transaxial spatial resolution of 2.3 mm in the center. Animals were scanned twice a day, first with ^{11}C-PiB, then 2 hours later with ^{18}F-BCPP-EF; the order of the tracers was not counterbalanced because of radiotracer half-life issues. Isoflurane at 1.5–2.0% in oxygen was used to anesthetize the mice for the duration of the entire scans. The animals were placed in the prone position on a fixation plate and were then set within the gantry hole of the PET scanner. After a 15-minute transmission scan using an external $^{68}Ge/^{68}Ga$ rod source (67 MBq) for attenuation correction, serial emission scans lasting for 70 min and 80 min were performed immediately following injections of ^{11}C-PiB at a dose of 8 MBq and ^{18}F-BCPP-EF at a dose of 5 MBq, respectively. The tracers were injected intravenously through a cannula inserted into the tail vein. No arterial sampling was conducted. The PET data were reconstructed using 3D DRAMA (iteration 2, gamma 0.1) with a Gaussian filter of 1.0 mm full width at half maximum (FWHM), yielding a voxel size of 0.65 × 0.65 × 1.0167 mm for the reconstructed images. To obtain anatomical information, X-ray CT scans were performed immediately following the PET measurements, using a ClairvivoCT (Shimadzu Corporation, Kyoto, Japan).

Immunohistochemistry

Immunostaining was performed as previously reported [14]. Briefly, mice were anesthetized with chloral hydrate (400 mg/kg) and transcardially perfused with phosphate-buffered saline (PBS) followed by 4% paraformaldehyde (PFA; pH 7.4). Their brains were removed, post-fixed in 4% PFA, and immersed in 30% sucrose in PBS as cryoprotectant until the tissue sank. Tissues were then frozen in dry ice and stored at −80 °C. Frozen coronal sections of 20-μm thickness were cut using a cryostat. The slides were blocked with 10% donkey serum in PBS containing 0.1% Triton X-100 for 1 hour at room temperature (RT), followed by incubation overnight at 4 °C with primary antibodies. After washing with PBS for three times, the slides were incubated for 1 hour at RT with fluorescent conjugated secondary antibodies. Then, they were washed three times with PBS and stained with DAPI to visualize nuclei. Fluorescent images of a single focal plane were obtained by confocal microscopy using a 63 × lens (SP8, Leica, Wetzlar, Germany). The following primary antibodies were used in this study: mouse anti-ATPB (1:200, Abcam, Tokyo, Japan), rabbit anti-CaMKII (1:500, Abcam), rabbit anti-GFAP (1:500, DAKO/Agilent, Santa Clara,

US), rabbit anti-Iba1 (1:500, WAKO, Saitama, Japan), and rat anti-PDGFRβ (1:250, kindly provided by Prof. Takakura, Osaka University). The secondary antibodies were as follows: Alexa Fluor 488 anti-rabbit IgG and anti-mouse IgG, Alexa Fluor 568 anti-rabbit IgG, Alexa Fluor 594 anti-mouse IgG, and Alexa Fluor 647 anti-goat IgG (1:500, Thermo Fisher Scientific, Waltham, USA).

Data and statistical analyses

The PET data were analyzed with PMOD image software (version 3.7; PMOD Technologies Ltd, Zurich, Switzerland). The SUVRs for ^{11}C-PiB and ^{18}F-BCPP-EF were estimated by dividing the target SUV by the cerebellar SUV, with the latter being taken to indicate the background level [8, 15]. The SUVs were calculated as the measured radioactivity divided by the ratio of the total injected dose to the mouse body weight. As described elsewhere [12, 16], ellipsoid volume of interest (nearly 2.9 mm x 0.8 mm x 1.5 mm in diameter) ranging from 14 to 16 mm^3 were placed over the frontal cortex anteriorly under the Bregma by referring to the X-ray CT images [12] (Supplementary Fig. 1). One-way analysis of variance (ANOVA) was performed to compare tracer uptake and mouse age, with the significance level set at $p < 0.05$ with a correction for multiple comparisons. Within each age group, correlation analysis was performed between the two tracer SUVRs (^{11}C-PiB SUVR and ^{18}F-BCPP-EF SUVR, at either 5 or 15 weeks-of-age) using the false discovery rate (FDR) correction for multiple correlations ($p < 0.05$), to examine deviations in patterns of the parameters in the living brains of SAMP10 mice in relation to the progression of senescence.

Results

PET findings

We first analyzed the mitochondrial activity in the brains of SAMR1 mice at 15 weeks-of-age and SAMP10 mice at 5 and 15 weeks-of-age using ^{18}F-BCPP-EF. Figure 1 shows the parametric PET images of ^{18}F-BCPP-EF uptake superimposed on CT images of 15-week-old SAMR1 mice (A) and 5-week-old (B) and 15-week-old (C) SAMP10 mice. The SUVRs of ^{18}F-BCPP-EF in the brain did not show a significant difference between SAMR1 mice and 5-week-old SAMP10 mice (Table 1). By contrast, in 15-week-old SAMP10 mice, the SUVR was higher throughout the brain (Fig. 1C), being significantly higher than that of the 5-week-old SAMP10 mice (Fig. 2A), meaning that mitochondrial oxidative metabolism had increased in the SAMP10 mice around the period of 15 weeks-of-age. Next, we analyzed the Aβ level using ^{11}C-PiB. The SUVRs of the control SAMR1 mice and 5-week-old SAMP10 mice did not show a significant difference (Fig. 1D-E and Fig. 2B). By contrast, the 15-week-old SAMP10 mice (Fig. 1F) showed a significantly higher ^{11}C-PiB SUVR than the 5-week-old mice (Fig. 2B), indicating that Aβ accumulation is detectable by PET at around 15 weeks of age. The lack of a significant difference between the 15-week-old SAMP10 and SAMR1 mice was due to a large variation in the ^{11}C-PiB SUVR in the SAMR1 mice. Direct comparisons between the ^{18}F-BCPP-EF and ^{11}C-PiB SUVRs showed a significant negative correlation in 15-week-old SAMP10 mice, but no significant correlation in either 5-week-old SAMP10 or 15-

week-old SAMR1 mice. This finding indicates that a greater Aβ burden reduces mitochondrial availability in 15-week-old SAMP10 mice, and *vice versa*.

Table 1
Differences in the SUVRs of 18F-BCPP-EF and 11C-PiB in the cortex

Group	week	^{18}F-BCPP-EF	^{11}C-PiB
SAMP10	5	0.87±0.03	0.92±0.09
	15	0.93±0.04*	1.187±0.15**
SAMPR1	15	0.80±0.06	0.96±0.23

* p<0.05 vs SAMPR1 (FDR corrected)
** p<0.05 vs SAMP10 at 5 weeks (FDR corrected)

Immunohistochemical findings

The PET finding of increased mitochondrial activity at 15 weeks-of-age in SAMP10 mice was followed by a confirmatory examination using immunohistochemical analyses. Double immunostaining against ATPB (a component of ATP synthase on the mitochondrial inner membrane) and CaMKII (a marker for neurons) was performed. In the control mice (15-week-old SAMR1 mice and 5-week-old SAMP10 mice), there were a small number of ATPB positive signals in the soma of neurons in the cerebral cortex (Fig. 3A-F). By contrast, in the 15-week-old SAMP10 mice, the intensity and numbers of ATPB-positive signals were dramatically elevated (Fig. 3G-I), which was consistent with the ^{18}F-BCPP-EF PET finding. The immuno-positive punctuate signals were observed not only in the soma, but also in neurites. This result suggests that neurons are poised to increase ATP production in the early stage of neurodegeneration.

As ATPB immuno-positive signals were also observed in non-neuronal cells, as shown in Fig. 3G, we next analyzed the localization of ATPB in astrocytes. In 15-week-old SAMR1 mice, the GFAP signal was mainly observed in the endfeet of perivascular astrocytes in the cerebral cortex (Fig. 4A-C), where we also found that ATPB was localized. While the ATPB immuno-positive signal was very low in 5-week-old SAMR1 mice (Fig. 4D-F), both the ATPB signal and the overall GFAP signal were much higher throughout the cerebral cortex in the 15-week-old SAMP10 mice, indicating proliferation of reactive astrocytes consistent with previous reports (Fig. 4G-I, data not shown) [17]. As expected, the ATPB signal was colocalized within the GFAP + astrocytes. Further analysis of the upregulation of ATPB in pericytes was performed, because many ATPB immuno-positive signals were found along a capillary (Supplementary Fig. 2), and progressive pericyte loss in a mouse model of AD pathogenesis was previously reported [18]. However, most of the ATPB signals along the capillary were located in astrocytes, not in pericytes (Supplementary Fig. 2).

Figure 5 shows the results of investigations into whether ATPB was localized to microglia. In the control mice (15-week-old SAMR1 and 5-week-old SAMP10 mice), the intensities of the ATPB immuno-positive signals were too weak to detect in Iba1 + microglia. By contrast, a detectable level of ATPB-positive signal

was colocalized with Iba1 + microglia in the 15-week-old SAMP10 mice. The microglia in these 15-week-old SAMP10 mice may have been protective microglia, as we recently reported that CB2 + microglia activation was dominant at an early stage of neurodegeneration [12]. Next, we analyzed the expression of TREM2, which reportedly has a protective function to prevent AD progression [19, 20]. While the TREM2 immuno-positive signal was very low in the microglia in the control mice (Fig. 6A–F), intensive TREM2 immuno-positive punctuate signals were observed in Iba1 + microglia in 15-week-old SAMP10 mice (Fig. 6G-I). This result supports our previous finding of the activation of protective microglia in SAMP10 mice at this early-stage, which is comparable to the state of senescence in early-stage MCI in humans.

Discussion

Detection of mitochondrial activity and amyloid deposition in SAMP10 mice

In this study, we showed that the SUVRs of ^{18}F-BCPP-EF and ^{11}C-PiB in the cerebral cortex were significantly higher in 15-week-old SAMP10 mice than in control mice, and that these SUVRs were inversely correlated with each other in 15-week-old SAMP10 mice (Figs. 1 and 2). To our knowledge, this is the first study to report a change in mitochondrial activity in SAMP10 mice on *in vivo* PET imaging, highlighting elevated mitochondrial activity at an early stage in SAMP10 mice, comparable to the early stage of AD spectrum disorder in humans. Although many researchers have investigated frontal lobe atrophy and Aβ-deposition using SAMP10 mice older than 7 months, we here used younger mice to analyze early molecular changes at the beginning of neurodegeneration. Aβ-deposition was not obvious at 5 weeks-of-age, but we did observe an elevation in the SUVR of ^{11}C-PiB in 15-week-old SAMP10 mice. As the SUVR of ^{18}F-BCPP-EF, which reflects oxidative phosphorylation in mitochondria, was also increased at the same stage (Figs. 1 and 2), it is probable that metabolism had increased to compensate for an energy loss in neurons, which happens with mitochondrial dysfunction in the pathological condition of Aβ-deposition in the AD brain. Although the pathological process is different, this compensatory theory is in line with previous reports of elevated dopamine synthesis in early Parkinson's disease [21, 22]. Of course, in a later stage of disease, reduced energy production would occur in association with more serious pathological events, as neurodegeneration progresses [23, 24].

A previous metabolomic study showed a difference in the metabolic pathway between MCI and AD patients [25], with the level of pyruvate in cerebrospinal fluid being significantly higher in MCI patients than in cognitively normal (CN) individuals and AD patients. It is also reported that gene expression of complex I-V subunits in the electron transport chain is elevated in MCI compared with AD and age-matched CN individuals [26]. Thus, the increase in mitochondrial activity in 15-week-old SAMP10 mice in the current study may reflect these changes in energy metabolism found in the state of senescence to MCI.

A Possible Key Player: Glial Cells

A possible key event that might be at play in the inverse correlation between Aβ deposition and mitochondrial activity is neuroinflammation, specifically neuroprotective glial activation. Aβ accumulation affects neurons and neuroinflammatory cells, and upregulation of IL-1β and IFN-γ in 3-month-old SAMP10 mice, and IL-6 in later-stage SAMP10 mice, have been observed [27]. In our recent study, neuroprotective microglia were more dominant than neuroinflammatory microglia in the early stage of neurodegeneration in SAMP10 mice [12]. We showed that elevation of mitochondrial energy metabolism, or oxidative phosphorylation, occurred according to the progression of neurodegeneration (Figs. 1 and 2A). Although the high energy requirements of neurons means that they form a major contribution to the oxidative metabolism of the brain, glial cells are also responsible for some of the oxidative metabolism. The oxidative metabolism in microglia changes as symptoms progress. While induction of M1-type inflammatory microglia by lipopolysaccharide leads to a reduction of mitochondrial oxygen consumption and lactate production, these reductions are not caused by IL-4/IL-13, inducers of M2-type protective microglia [28]. This indicates the occurrence of higher metabolism in M2 type microglia. When protective microglia are dominant in the early stage of neurodegeneration, oxidative phosphorylation in mitochondria remains at a high level. However, as the number of protective microglia decreases and neuroinflammatory microglia become prominent with the progression of Aβ deposition in later stages, the oxidative phosphorylation activity in microglia will be reduced by mitochondrial dysfunction, concomitant with that in neurons [28].

Interaction Of Amyloid And Neuronal Mitochondria

One of the mechanisms by which amyloid leads to mitochondrial dysfunction is the transportation of APP into mitochondria [29]. Pre-sequence protein (PreP), a processing enzyme that recognizes mitochondrial-targeting signal peptides and cleaves after protein import, can degrade Aβ in the mitochondria [30]. Interestingly, the proteolytic activity of PreP is decreased in the AD brain [31]. Aβ can be localized to the inner mitochondrial membrane [32], and constituents of the γ-secretase complex, such as nicastrin, APH-1, PEN-2, and presenilin-1, which function in APP processing, are also localized within the mitochondria-associated membrane [33, 34]. It has been reported that mitochondrial dysfunction and neurodegeneration occur in model mice with deleted HtrA2, a serine protease that interacts with Aβ, APP, and presenilin-1 within the intermembrane space [35]. These pieces of evidence suggest that Aβ and Aβ-related enzymes are linked with failure of mitochondrial function.

Immunohistochemical Confirmation

Our immunohistochemical analyses presented in Figs. 3 to 5 show that in 15-week-old SAMP10 mice, mitochondrial ATPB, a key enzyme for ATP production, was mainly present in neurons, although some was present in microglia, and slightly elevated levels were also present in reactive/perivascular

astrocytes. Because the population of neurons was most abundant in the cerebral cortex and upregulation of ATPB in neuron was prominent compared to astrocytes and microglia, the primary contributor to the higher SUVR of ^{18}F-BCPP-EF in the 15-week-old SAMP10 mice was considered to be neurons. As the number of GFAP + reactive astrocytes in the cortex had increased (data not shown) [17], and specific CB2 + protective microglia were activated at this early stage in the SAMP10 mice [12], we speculate that the extent of the polarized neuroinflammatory responses (neurotoxic or neuroprotective) of these glial cells would be of relevance to future neuronal degeneration. The protective cytokines (including neurotrophic factors) that are released from microglia exposed to neuropathic substances such as Aβ might stimulate neurons to supply more glucose and glutamine from perivascular astrocytes. These supplies may enable neurons to survive by temporarily increasing energy production.

The blood-brain barrier breakdown caused by pericyte dysfunction and impairment of platelet-derived growth factor receptor-β (PDGFRβ) signaling have recently been attracting attention as pathological features of AD. Pericytes are involved in the efflux of accumulated Aβ in the brain. Originally, we thought that pericyte activity might be elevated at an early stage of neurodegeneration; however, in 15-week-old SAMP10 mice, there was no increase in the immunostaining level of ATPB in pericytes, while adjacent astrocytes contained a higher level of ATPB (Supplementary Fig. 2). In this relatively early stage animal model, the contribution of pericytes to accumulation of Aβ in the brain parenchyma may be minimal. Indeed, the number of pericytes starts to decrease after 4 months-of-age in 5xFAD mice [18].

We also observed elevation of TREM2 (an important protein for clearance of Aβ) in microglia in 15-week-old SAMP10 mice (Fig. 6). TREM2 is a key player in the switching of microglia from a homeostatic state to a disease-associated state. Interestingly, soluble TREM2 in cerebrospinal fluid is higher in Aβ + Tau + MCI patients than in CN individuals [36]. Furthermore, TREM2 expression in mononuclear cells in the peripheral blood of MCI patients, especially those likely to convert to AD, was significantly higher than in CN individuals [37]. TREM2 activates the mTOR pathway that regulates mitochondrial energy production by promoting the synthesis of mitochondrial proteins, including components of MC-1 and MC-5 [38]. Therefore, the correlation between mitochondrial activity and TREM2 expression is reasonable.

Conclusion

In this study, we found that the SUVRs of ^{18}F-BCPP-EF and ^{11}C-PiB were significantly higher in the brains of 15-week-old SAMP10 mice than in 5-week-old SAMP10 mice and 15-week-old SAMR1 mice, indicating an increase in mitochondrial activity and Aβ deposition occurring in the brain in the early state of senescence towards cognitive impairment and AD spectrum-type neurodegeneration. Interestingly, the SUVR of ^{18}F-BCPP-EF was negatively correlated with that of ^{11}C-PiB. Consistent with this PET analysis, we also found that ATPB was strongly upregulated, mainly in the neurons, in the cerebral cortex of 15-week-old SAMP10 mice, along with elevated activation of astrocytes and microglia. Hence, Aβ-induced neuroinflammation may shift the net production of ATP from neuronal oxidative metabolism to anaerobic glycolysis, as supported by the negative correlation between mitochondrial activity and Aβ accumulation.

This contention could lead to a therapeutic expectation that a specific treatment to sustain mitochondrial activity might help ameliorate senescence-related neuroinflammation and degeneration.

Limitations

There are several limitations of note in the current study. First, although we measured changes in the uptake of both ^{18}F-BCPP-EF and ^{11}C-PiB in 5- and 15-week-old SAMP10 mice and control SAMR1 mice, the PET data did not reveal the mitochondrial activities of any particular cell types: neurons, microglia, oligodendrocytes and/or astrocytes. As the present study focused on changes in early-stage SAMP10 mice, observations at a later stage might reveal different expression of inflammatory substances and cells; hence, a further study is needed to address this issue in the broader time course of senescence-related neuronal loss. Second, because the spatial resolution of the PET scanner used was only 2.3 mm, the results may be subject to partial volume effects. To reduce such effects, we tried to set the measurement VOIs to at least twice the size of the FWHM of the scanner. An alternative would be to use autoradiography instead of PET, although measures of parameter change within the same animal cannot be obtained using autoradiography. Third, as we did not make additional PET measurements using a tracer for neuroinflammation in the same animals, we could not evaluate the direct contribution of neuroinflammation to the change in mitochondrial activity. However, taking our recent PET results on neuroinflammation [12] into consideration, we consider an *in vivo* relationship to be likely, as mentioned above.

List Of Abbreviations

^{11}C-PiB = [^{11}C]Pittsburgh compound B; ^{18}F-BCPP-EF = [^{18}F]2-tert- butyl-4-chloro- 5–2H- pyridazin-3-one; Aβ = beta-amyloid; AD = Alzheimer's disease; ATPB = ATP synthase subunit beta; CN = cognitively normal; FDR = false discovery rate; FOV = field of view; FWHM = full width at half maximum; GFAP = Glial fibrillary acidic protein; MCI = mild cognitive impairment; PET = positron emission tomography; ROS = reactive oxygen species; SAMR1 = senescence-accelerated mouse resistant 1; SAMP10 = senescence-accelerated mouse prone 10; SUVR = standard uptake value ratios; VOI = Volume of interest

Declarations

Ethics approvaland consent to participate

All animal experiments were approved by the ethics committees of the Central Research Laboratory at Hamamatsu Photonics and Hamamatsu University School of Medicine. The approval reference number is 2015065.

Consent for publication

Not applicable. This study involves no human materials.

Availability of data and materials

The datasets supporting the conclusions of this article are available by request, but will not be posted on a repository at this point due to intellectual property/confidentiality issues.

Competing interests

The authors declare that they have no competing interests.

Funding

This work was supported by grants from JSPS KAKENHI (grant numbers 17K08512 (SY) and 17H04247(YO)), AMED (grant number JP19ek0109297 (YO), 19lm0203078h0001(SY)), a Grant-in-Aid for Scientific Research on Innovative Areas (grant number JP16H06402 (YO)), the Takeda Science Foundation (SY), and a HUSM Grant-in-Aid (SY).

Authors' contributions

SY and YO designed, analyzed, and wrote the paper. SY, YI, SI, and TK performed the research. SN, KM, and HT synthesized the tracers. HO and KS evaluated and advised on the design. All authors have seen and agree with the content of the manuscript.

Acknowledgments

The authors would like to thank Makiko Kato (Department of Organ and Tissue Anatomy, Hamamatsu University School of Medicine) and Dai Fukumoto (Central Research Laboratory, Hamamatsu Photonics KK) for their excellent support. We thank Prof. Nobuyuki Takakura and Dr. Hiroyasu Kidoya (Osaka University) for anti-PDGFRb antibody. Confocal imaging was obtained with the kind support of the Advanced Research Facilities and Services, Preeminent Medical Photonics Education and Research Center, Hamamatsu University School of Medicine.

References

1. Perez-Gracia E, Blanco R, Carmona M, Carro E, Ferrer I. Oxidative stress damage and oxidative stress responses in the choroid plexus in Alzheimer's disease. Acta Neuropathol. 2009;118:497–504. doi:10.1007/s00401-009-0574-4.

2. Lejri I, Agapouda A, Grimm A, Eckert A. Mitochondria- and Oxidative Stress-Targeting Substances in Cognitive Decline-Related Disorders: From Molecular Mechanisms to Clinical Evidence. Oxid Med Cell Longev. 2019;2019:9695412. doi:10.1155/2019/9695412.
3. Petersen RC. Mild cognitive impairment as a diagnostic entity. J Intern Med. 2004;256:183–94. doi:DOI 10.1111/j.1365-2796.2004.01388.x.
4. Morris JC. Revised criteria for mild cognitive impairment may compromise the diagnosis of Alzheimer disease dementia. Arch Neurol. 2012;69:700–8. doi:10.1001/archneurol.2011.3152.
5. Hatashita S, Wakebe D. Amyloid-beta Deposition and Long-Term Progression in Mild Cognitive Impairment due to Alzheimer's Disease Defined with Amyloid PET Imaging. Journal of Alzheimers Disease. 2017;57:765–73. doi:10.3233/Jad-161074.
6. Harada N, Nishiyama S, Kanazawa M, Tsukada H. Development of novel PET probes, [18F]BCPP-EF, [18F]BCPP-BF, and [11C]BCPP-EM for mitochondrial complex 1 imaging in the living brain. J Label Compd Radiopharm. 2013;56:553–61. doi:10.1002/jlcr.3056.
7. Tsukada H, Nishiyama S, Fukumoto D, Kanazawa M, Harada N. Novel PET probes 18F-BCPP-EF and 18F-BCPP-BF for mitochondrial complex I: a PET study in comparison with 18F-BMS-747158-02 in rat brain. J Nucl Med. 2014;55:473–80. doi:10.2967/jnumed.113.125328.
8. Terada T, Obi T, Bunai T, Matsudaira T, Yoshikawa E, Ando I, et al. In vivo mitochondrial and glycolytic impairments in patients with Alzheimer disease. Neurology. 2020. doi:10.1212/WNL.0000000000009249.
9. Higuchi K. Genetic characterization of senescence-accelerated mouse (SAM). Exp Gerontol. 1997;32:129–38. doi:10.1016/s0531-5565(96)00060-5.
10. Shimada A, Tsuzuki M, Keino H, Satoh M, Chiba Y, Saitoh Y, et al. Apical vulnerability to dendritic retraction in prefrontal neurones of ageing SAMP10 mouse: a model of cerebral degeneration. Neuropathol Appl Neurobiol. 2006;32:1–14. doi:10.1111/j.1365-2990.2006.00632.x.
11. Hasegawa-Ishii S, Takei S, Chiba Y, Furukawa A, Umegaki H, Iguchi A, et al. Morphological impairments in microglia precede age-related neuronal degeneration in senescence-accelerated mice. Neuropathology. 2011;31:20–8. doi:10.1111/j.1440-1789.2010.01126.x.
12. Yamagishi S, Iga Y, Nakamura M, Takizawa C, Fukumoto D, Kakiuchi T, et al. Upregulation of cannabinoid receptor type 2, but not TSPO, in senescence-accelerated neuroinflammation in mice: a positron emission tomography study. J Neuroinflammation. 2019;16:208. doi:10.1186/s12974-019-1604-3.
13. Klunk WE, Engler H, Nordberg A, Wang Y, Blomqvist G, Holt DP, et al. Imaging brain amyloid in Alzheimer's disease with Pittsburgh Compound-B. Ann Neurol. 2004;55:306–19. doi:10.1002/ana.20009.
14. Yamagishi S, Yamada K, Sawada M, Nakano S, Mori N, Sawamoto K, et al. Netrin-5 is highly expressed in neurogenic regions of the adult brain. Front Cell Neurosci. 2015;9. doi:10.3389/fncel.2015.00146.

15. Manook A, Yousefi BH, Willuweit A, Platzer S, Reder S, Voss A, et al. Small-animal PET imaging of amyloid-beta plaques with [11C]PiB and its multi-modal validation in an APP/PS1 mouse model of Alzheimer's disease. PLoS One. 2012;7:e31310. doi:10.1371/journal.pone.0031310.
16. Ouchi Y, Tsukada H, Kakiuchi T, Nishiyama S, Futatsubashi M. Changes in cerebral blood flow and postsynaptic muscarinic cholinergic activity in rats with bilateral carotid artery ligation. J Nucl Med. 1998;39:198–202.
17. Kawamata T, Akiguchi I, Maeda K, Tanaka C, Higuchi K, Hosokawa M, et al. Age-related changes in the brains of senescence-accelerated mice (SAM): association with glial and endothelial reactions. Microsc Res Tech. 1998;43:59–67. doi:10.1002/(SICI)1097-0029(19981001)43:1<59::AID-JEMT9>3.0.CO;2-X.
18. Giannoni P, Arango-Lievano M, Neves ID, Rousset M-C, Baranger K, Rivera S, et al. Cerebrovascular pathology during the progression of experimental Alzheimer's disease. Neurobiology of Disease. 2016;88:107–17. doi:10.1016/j.nbd.2016.01.001.
19. Ulland TK, Colonna M. TREM2 — a key player in microglial biology and Alzheimer disease. Nature Reviews Neurology. 2018;14:667–75. doi:10.1038/s41582-018-0072-1.
20. 10.1016/j.cell.2017.07.023
Ulland TK, Song WM, Huang SC, Ulrich JD, Sergushichev A, Beatty WL, et al. TREM2 Maintains Microglial Metabolic Fitness in Alzheimer's Disease. Cell. 2017;170:649 – 63 e13. doi:10.1016/j.cell.2017.07.023.
21. Doudet DJ, Chan GL, Holden JE, McGeer EG, Aigner TA, Wyatt RJ, et al. 6-[18F]Fluoro-L-DOPA PET studies of the turnover of dopamine in MPTP-induced parkinsonism in monkeys. Synapse. 1998;29:225–32. doi:10.1002/(SICI)1098-2396(199807)29:3<225::AID-SYN4>3.0.CO;2-8.
22. Kaasinen V, Nurmi E, Bruck A, Eskola O, Bergman J, Solin O, et al. Increased frontal [(18)F]fluorodopa uptake in early Parkinson's disease: sex differences in the prefrontal cortex. Brain. 2001;124:1125–30. doi:10.1093/brain/124.6.1125.
23. Perkins M, Wolf AB, Chavira B, Shonebarger D, Meckel JP, Leung L, et al. Altered Energy Metabolism Pathways in the Posterior Cingulate in Young Adult Apolipoprotein E varepsilon4 Carriers. J Alzheimers Dis. 2016;53:95–106. doi:10.3233/JAD-151205.
24. Valla J, Yaari R, Wolf AB, Kusne Y, Beach TG, Roher AE, et al. Reduced posterior cingulate mitochondrial activity in expired young adult carriers of the APOE epsilon4 allele, the major late-onset Alzheimer's susceptibility gene. J Alzheimers Dis. 2010;22:307–13. doi:10.3233/JAD-2010-100129.
25. Trushina E, Dutta T, Persson XMT, Mielke MM, Petersen RC. Identification of Altered Metabolic Pathways in Plasma and CSF in Mild Cognitive Impairment and Alzheimer's Disease Using Metabolomics. Plos One. 2013;8. doi:UNSP e63644.
26. 1371/journal.pone.0063644.
27. Berchtold NC, Sabbagh MN, Beach TG, Kim RC, Cribbs DH, Cotman CW. Brain gene expression patterns differentiate mild cognitive impairment from normal aged and Alzheimer's disease. Neurobiol Aging. 2014;35:1961–72. doi:10.1016/j.neurobiolaging.2014.03.031.

28. Kumagai N, Chiba Y, Hosono M, Fujii M, Kawamura N, Keino H, et al. Involvement of pro-inflammatory cytokines and microglia in an age-associated neurodegeneration model, the SAMP10 mouse. Brain Res. 2007;1185:75–85. doi:10.1016/j.brainres.2007.09.021.
29. Orihuela R, McPherson CA, Harry GJ. Microglial M1/M2 polarization and metabolic states. Br J Pharmacol. 2016;173:649–65. doi:10.1111/bph.13139.
30. Anandatheerthavarada HK, Biswas G, Robin MA, Avadhani NG. Mitochondrial targeting and a novel transmembrane arrest of Alzheimer's amyloid precursor protein impairs mitochondrial function in neuronal cells. J Cell Biol. 2003;161:41–54. doi:10.1083/jcb.200207030.
31. Falkevall A, Alikhani N, Bhushan S, Pavlov PF, Busch K, Johnson KA, et al. Degradation of the amyloid beta-protein by the novel mitochondrial peptidasome, PreP. J Biol Chem. 2006;281:29096–104. doi:10.1074/jbc.M602532200.
32. Alikhani N, Guo L, Yan S, Du H, Pinho CM, Chen JX, et al. Decreased proteolytic activity of the mitochondrial amyloid-beta degrading enzyme, PreP peptidasome, in Alzheimer's disease brain mitochondria. J Alzheimers Dis. 2011;27:75–87. doi:10.3233/JAD-2011-101716.
33. Manczak M, Anekonda TS, Henson E, Park BS, Quinn J, Reddy PH. Mitochondria are a direct site of A beta accumulation in Alzheimer's disease neurons: implications for free radical generation and oxidative damage in disease progression. Hum Mol Genet. 2006;15:1437–49. doi:10.1093/hmg/ddl066.
34. Del Prete D, Suski JM, Oules B, Debayle D, Gay AS, Lacas-Gervais S, et al. Localization and Processing of the Amyloid-beta Protein Precursor in Mitochondria-Associated Membranes. J Alzheimers Dis. 2017;55:1549–70. doi:10.3233/JAD-160953.
35. Hansson CA, Frykman S, Farmery MR, Tjernberg LO, Nilsberth C, Pursglove SE, et al. Nicastrin, presenilin, APH-1, and PEN-2 form active gamma-secretase complexes in mitochondria. J Biol Chem. 2004;279:51654–60. doi:10.1074/jbc.M404500200.
36. Patterson VL, Zullo AJ, Koenig C, Stoessel S, Jo H, Liu X, et al. Neural-specific deletion of Htra2 causes cerebellar neurodegeneration and defective processing of mitochondrial OPA1. PLoS One. 2014;9:e115789. doi:10.1371/journal.pone.0115789.
37. Ewers M, Franzmeier N, Suarez-Calvet M, Morenas-Rodriguez E, Caballero MAA, Kleinberger G, et al. Increased soluble TREM2 in cerebrospinal fluid is associated with reduced cognitive and clinical decline in Alzheimer's disease. Science Translational Medicine. 2019;11. doi:ARTN eaav6221.
38. 1126/scitranslmed.aav6221.
39. Casati M, Ferri E, Gussago C, Mazzola P, Abbate C, Bellelli G, et al. Increased expression of TREM2 in peripheral cells from mild cognitive impairment patients who progress into Alzheimer's disease. Eur J Neurol. 2018;25:805–10. doi:10.1111/ene.13583.
40. Morita M, Gravel SP, Hulea L, Larsson O, Pollak M, St-Pierre J, et al. mTOR coordinates protein synthesis, mitochondrial activity and proliferation. Cell Cycle. 2015;14:473–80. doi:10.4161/15384101.2014.991572.

Figures

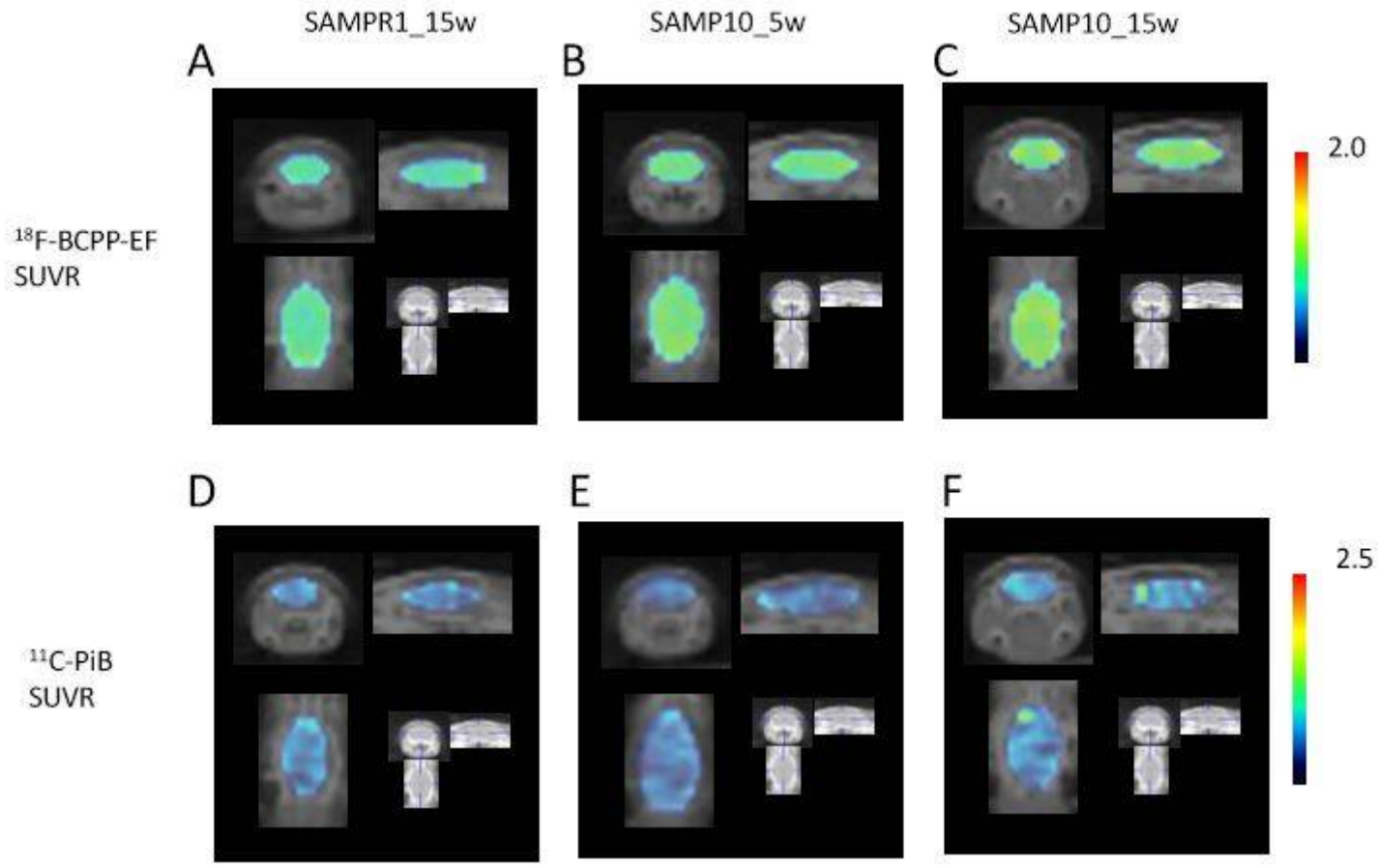

Figure 1

Parametric PET images of 18F-BCPP-EF (upper panels) and 11C-PiB (lower panels) tracers in 15-week-old SAMR10 mice (A), and 5-week old (B) and 15-week-old (C) SAMP10 mice. The PET data are superimposed on X-ray CT images, and the color bar denotes the SUVR.

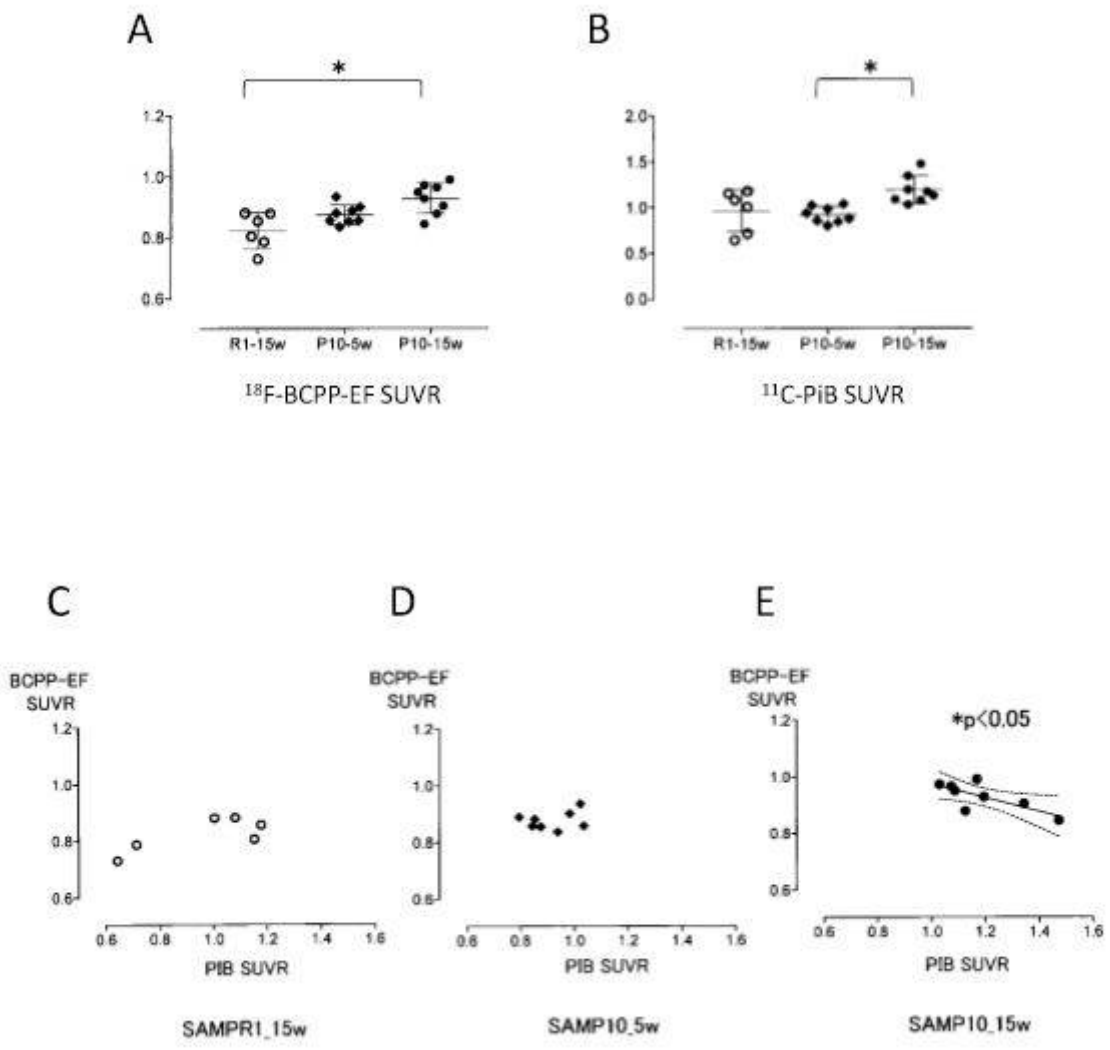

Figure 2

The SUVRs of 18F-BCPP-EF (A) and 11C-PiB (B) tracers and the relationships between them (C-E). The 18F-BCPP-EF and 11C-PiB (B) SUVRs were significantly higher in the 15-week-old SAMP10 mice than in the controls (A and B, *p < 0.05). A negative correlation between the binding of the two tracers was found in the 15-week-old SAMP10 mice (E). The dotted lines in (E) represent the 95% confidence intervals for the correlation.

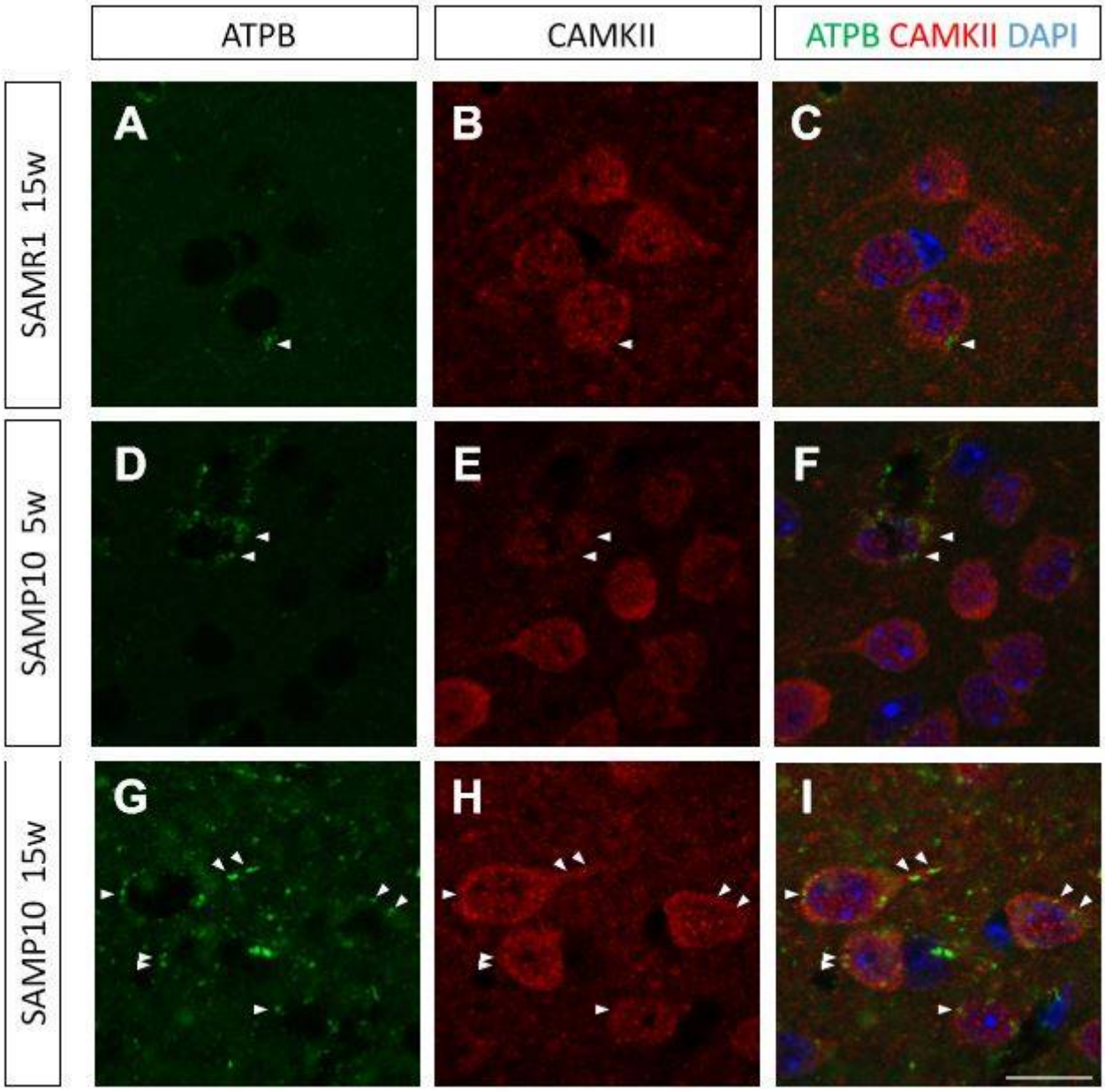

Figure 3

Double immunostaining for ATPB (green) and CaMKII (red) in the cerebral cortex of 15-week-old SAMR1 mice (A-C) and 5-week-old (D-F) and 15-week-old (G-I) SAMP10 mice. Note that the ATPB signal had greatly increased and was localized to the neurons at 15-weeks-of-age. Arrowheads indicate ATPB signals. Scale bar: 10 μm.

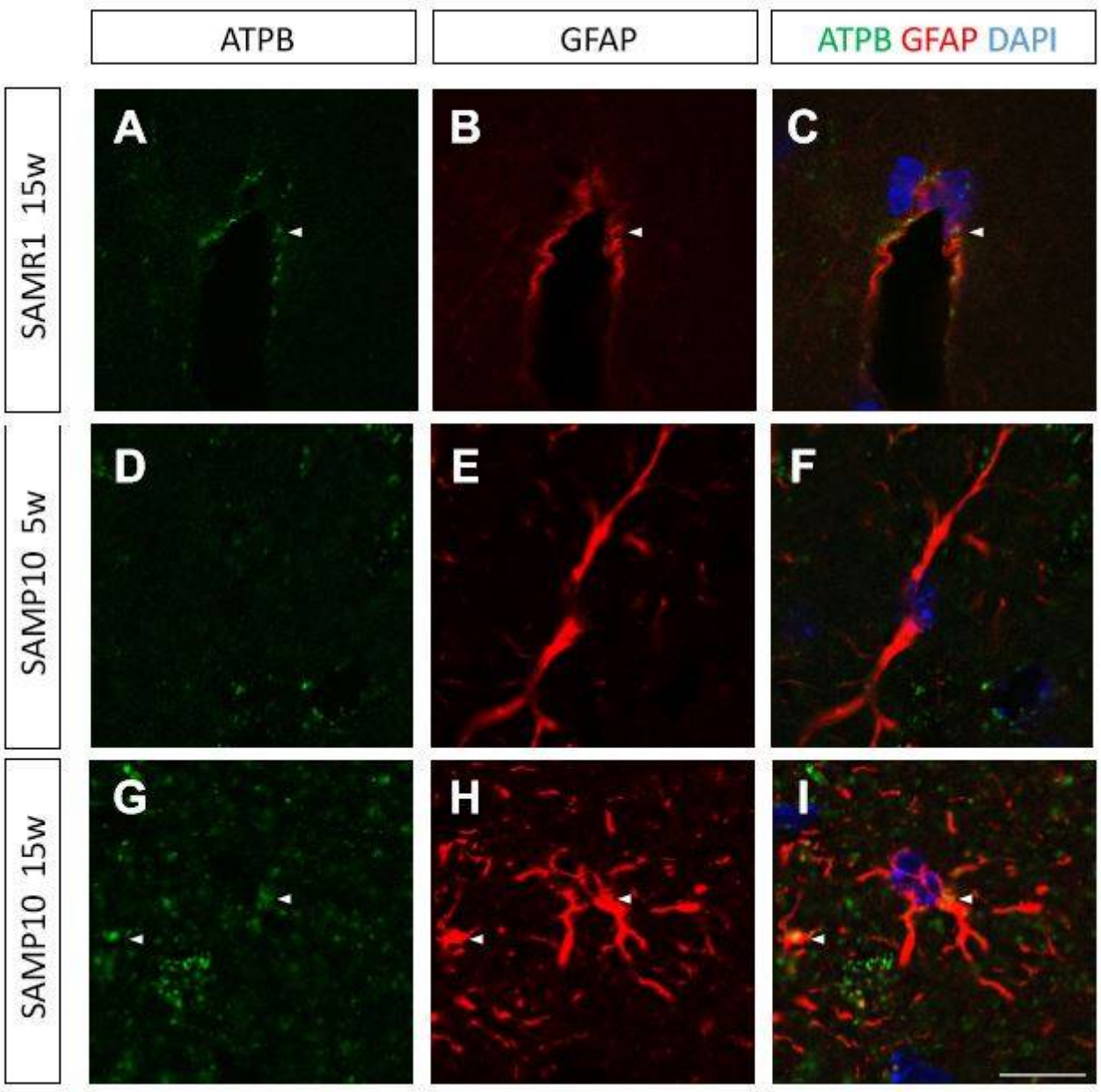

Figure 4

Immunostaining for ATPB (green) and GFAP (red) in the cerebral cortex of 15-week-old SAMR1 mice (A-C) and 5-week old (D-F) and 15-week-old (G-I) SAMP10 mice. Note that both ATPB and GFAP immuno-reactivity were much higher in the 15-week-old SAMP10 mice than in the two control groups. The localization of ATPB was observed in GFAP+ astrocytes. Arrowheads indicate ATPB signals. Scale bar: 10 μm.

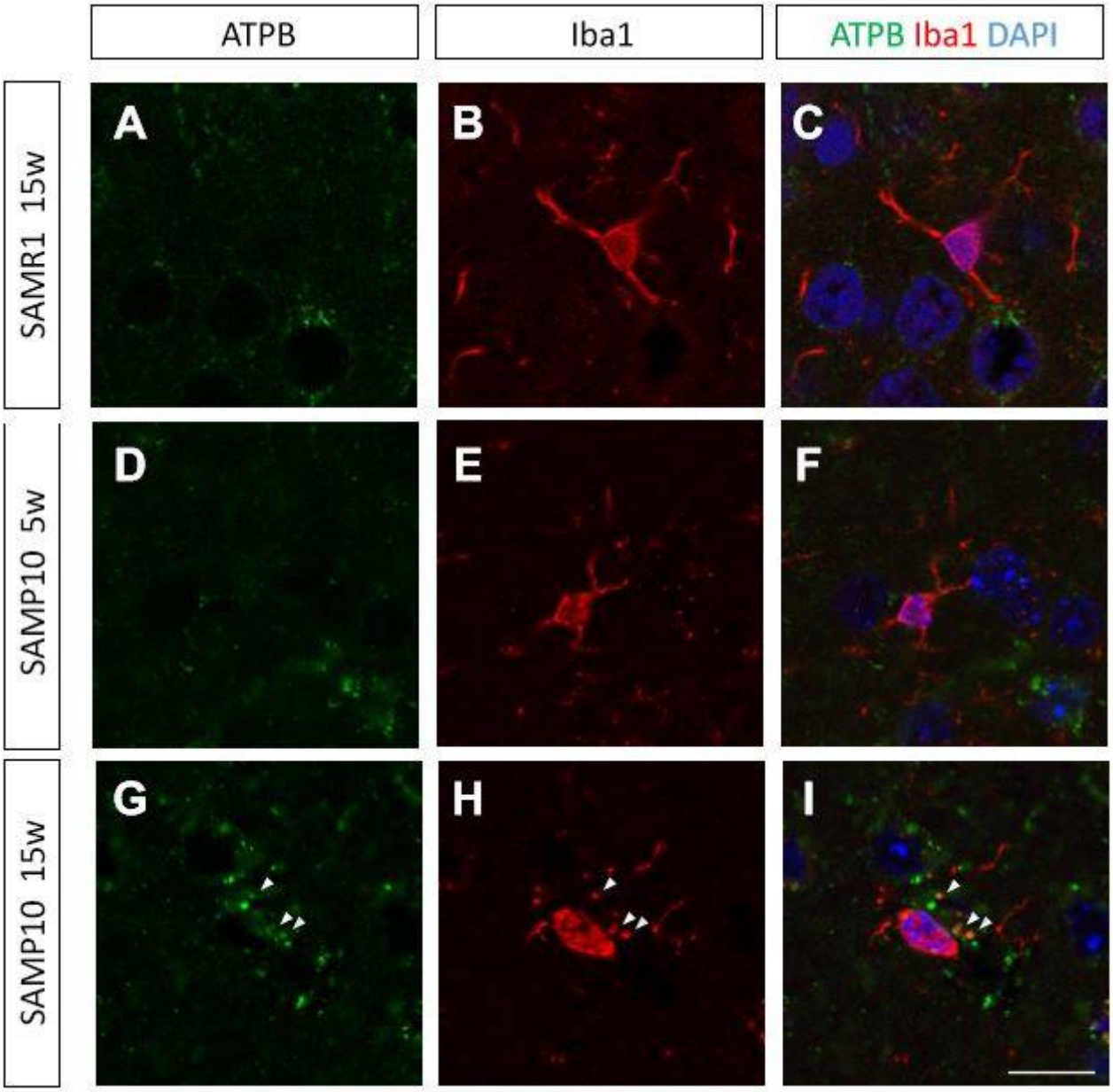

Figure 5

Double immunostaining for ATPB (green) and Iba1 (red) in the cerebral cortex of 15-week-old SAMR1 mice (A-C) and 5-week old (D-F) and 15-week-old (G-I) SAMP10 mice. Note that the ATPB signal was much higher and localized to the microglia in the 15-week-old SAMP10 mice. Arrowheads indicate ATPB signals. Scale bar: 10 μm.

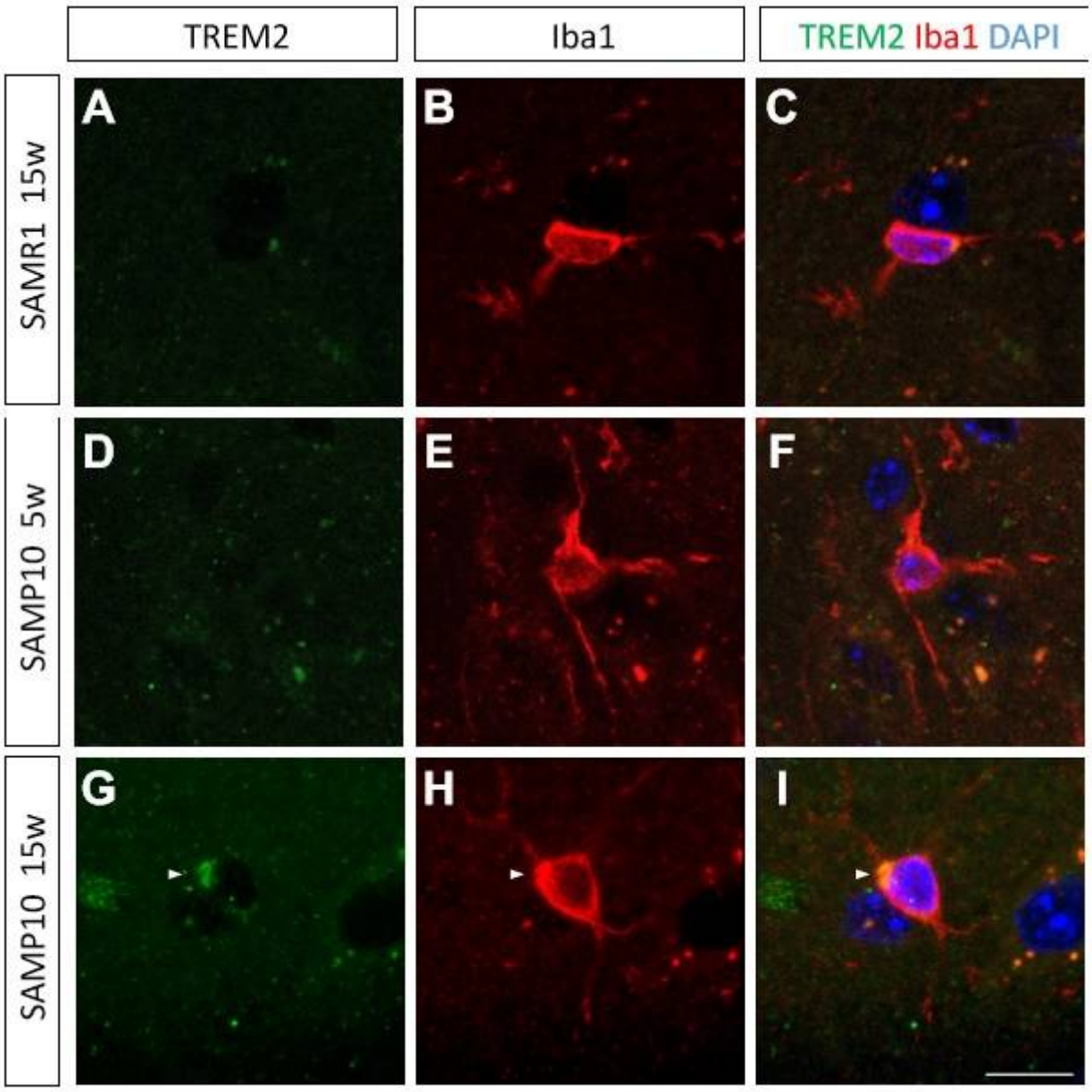

Figure 6

Immunostaining for TREM2 (green) and Iba1 (red) in the cerebral cortex of 15-week-old SAMR1 mice (A-C) and 5-week-old (D-F) and 15-week-old (G-I) SAMP10 mice. Note that TREM2 immuno-reactivity was higher and localized to the microglia in the 15-week-old SAMP10 mice. Arrowheads indicate TREM2 signals. Scale bar: 10 μm.

Supplementary Files

This is a list of supplementary files associated with this preprint. Click to download.

- supFigure1BCPPEFPIBpaper20200507.pdf
- supFigure2BCPPEFPIBpaper20200507.pdf

- SUPPLEMENTARYFIGURE12.docx